Ionics (2020) 26:1721–1728
https://doi.org/10.1007/s11581-019-03391-w

ORIGINAL PAPER

# Single-walled carbon nanotube as conductive additive for SiO/C composite electrodes in pouch-type lithium-ion batteries

Xin-ming Fan [1,2] · Xia-hui Zhang [3] · Guo-rong Hu [1,2] · Bao Zhang [1,2] · Zhen-jiang He [1,2] · Yun-jiao Li [1] · Jun-chao Zheng [1,2]

Received: 27 October 2019 / Revised: 28 November 2019 / Accepted: 1 December 2019 / Published online: 24 December 2019


## Abstract

SiO/C is believed to be one of the most promising anode material for lithium-ion batteries due to the low operation potential and superior theoretical capacity. However, the substantial volume change during cycling process limits its further practical application. Herein, we report an affordable and highly effective approach to enhancing the electrochemical performance by adding a small amount of single-walled carbon nanotubes (SWCNT) as conductive additive for SiO/C anodes. An efficient liquid-phase mixing approach is employed to evenly disperse the SWCNT into silicon oxide/graphite composite anode for lithium-ion batteries (LIBs). The electrochemical capability is carried out using pouch full cells with commercial electrode areal loading and mass loading. The addition of SWCNT (0.5%) reduces film resistance and direct current resistance (DCR) for charging. The lithium-ion diffusion coefficient is $6.32 \times 10^{-15}$ $cm^2$ $s^{-1}$ for SWCNT-added sample, which is an order of magnitude higher than that of the sample without SWCNT ($2.33 \times 10^{-16}$ $cm^2$ $s^{-1}$). Furthermore, the battery assembled by the SWCNT-adding electrode shows better rate performance and cycle stability. The charge efficiency improves 1.25 times at 4 C charging, which enables fast charging for LIBs. The cycling results show that SWCNT-adding electrode displays capacity retention of 90.30% after 600 cycles at 1 C. Furthermore, the loading of SiO/C electrode increases from 93.4 to 95.4 wt%, which is beneficial for improvement of energy density. It is worth noting that it suggests a well-designed recipe for the practical application of SWCNT for LIBs.

**Keywords** Lithium-ion batteries · Silicon oxide/graphite composite · Single-walled carbon nanotube · Conductive additive

## Introduction

With the rapid development and implementation of consumer electronics devices and electric vehicles, tremendous efforts have been stimulated towards pursuing high energy density and long cycle life of rechargeable lithium-ion batteries (LIBs) to satisfy the soaring demands [1–9]. The conventional graphite anode, due to its limited theoretical capacity (372 mAh $g^{-1}$), could not meet the increasing demand for high energy density [10]. Therefore, researchers are dedicated to exploring alternative anode active materials with a high reversible capacity [11, 12]. Among extensively studied next-generation anodes, silicon has been considered as one of the most attractive candidates owing to its superior theoretical specific capacity (4200 mAh $g^{-1}$), which is approximately ten times larger than that of conventional graphite, and a low charge potential (< 0.5 V vs. $Li^+$/Li) [13, 14]. To better couple with commercial cathodes, such as $LiCoO_2$ and $Li(Ni_{1-x-y}Co_xMn_y)O_2$, the silicon oxide/graphite (SiO/C) composite anode with a proportion of Si is recognized as promising negative materials for commercial application in LIBs. However, the large-scale commercial application of SiO/C has been impeded by low electron conductivity and large volume expansion during lithiation and delithiation process [15, 16]. Furthermore, the conductivity of electrode is further decreased when the SiO/C anode materials are combined with binders that are generally electronical insulators. Therefore, significant research effort is dedicated to enhance the conductivity of SiO/C anodes. The conductive additive is one of the most

**Electronic supplementary material** The online version of this article (https://doi.org/10.1007/s11581-019-03391-w) contains supplementary material, which is available to authorized users.

✉ Jun-chao Zheng
jczheng@csu.edu.cn

[1] School of Metallurgy and Environment, Central South University, Changsha 410083, Hunan, China

[2] National Engineering Laboratory for High Efficiency Recovery of Refractory Nonferrous Metals, Changsha 410083, China

[3] School of Mechanical and Materials Engineering, Washington State University, Pullman, WA 99164, USA

promising and practical approaches. However, the conductive additive does not contribute to the energy density, and thus, its adding amount needs to be optimized to achieve good conductivity and decent volumetric energy density.

Super P (SP) is believed to be one of the most widely used conductive additives and recognized as zero-dimensional particles (0D) that easily form aggregates. Meanwhile, it provides inefficient electronic pathways due to "point-to-point" contact. In this regard, a large amount of SP particles are required in the electrode formulations to achieve relatively high conductive efficiency [17, 18]. Unlike 0D SP, carbon nanotube (CNT), in particular SWCNT, is one-dimensional (1D) material with high porosity and high surface area, which is considered as an attractive conductive addition agent [19, 20]. As shown in Fig. 1, the 1D CNTs form three-dimensional (3D) conductive nets by the efficient "line-to-line" contact between other CNTs and active material particles. Therefore, numerous efforts have been directed at improving these issues using CNT conductive additive. Lim et al. reported that carbon nanotube can improve cycling performance for anode materials compared with carbon black conductive additive [21]. Sheem et al. reported that the resistivity of electrode using CNTs was one order magnitude lower than that of super P electrode [22, 23]. Nevertheless, these scientific investigations have been only evaluated for coin cells.

In this work, we report the effect of SWCNT as a conductive additive on the performance of SiO/C anodes. The SWCNT 3D conductivity networks were found to be well covered all the SiO/C primary particles. The prepared SWCNT-SiO/C composites were electrochemically investigated as the anode electrode in full pouch cells with $LiNi_{0.80}Co_{0.10}Mn_{0.10}O_2$ (LNCM) as the cathode material. Their electrochemical performances including charge-discharge rate and cycle performance were systematically investigated.

## Experimental

### Electrode preparation

To prepare the SiO/C@SWCNT electrodes, the SWCNT powders (90%, Aladdin) were uniformly dispersed in polyvinyl pyrrolidone (PVP, Aladdin) and $H_2O$ (DI water) solution to form the SWCNT suspension. The aqueous slurry, containing SiO/C anode materials (BTR New Energy Material Ltd), super P and SWCNT conductive additive, and polymer binder, was mixed and dispersed in a double high-speed disperse mixer. For control sample, the composite with only conventional SP as the conductive additive was prepared. The chemical composition of each anode for this work is listed in Table 1. The anode slurry was evenly coated on copper current collector with a pilot-scale slot-die coater. As for cathode fabrication, the electrodes were prepared by mixture slurry of $LiNi_{0.80}Co_{0.10}Mn_{0.10}O_2$ active material (96.4 wt%), carbon black (2.3 wt%), and PVDF (1.3 wt%). The corresponding slurry was carefully coated on an aluminum foil substrate with automatic coating machine. The areal loading of anode and cathode is around 21.2 mg $cm^{-2}$ (ca. 9.54 mAh $cm^{-2}$) and 47.0 mg $cm^{-2}$ (ca. 8.46 mAh $cm^{-2}$), respectively. The design capacity of anode and cathode is 450 mAh $g^{-1}$ and 180 mAh $g^{-1}$, respectively. The capacity balance of anode/cathode was approximately 1.1 for pouch cells.

### Material characterization

The morphology of materials and as-prepared electrodes was performed through field-emission scanning electron microscopy (FESEM, JSM 6400, JEOL). The film resistance of anode electrode was characterized using a two-probe approach [24]. Two high-conductivity probing system (ACCFILM Technology Co., Ltd.) was used to test the film resistance of

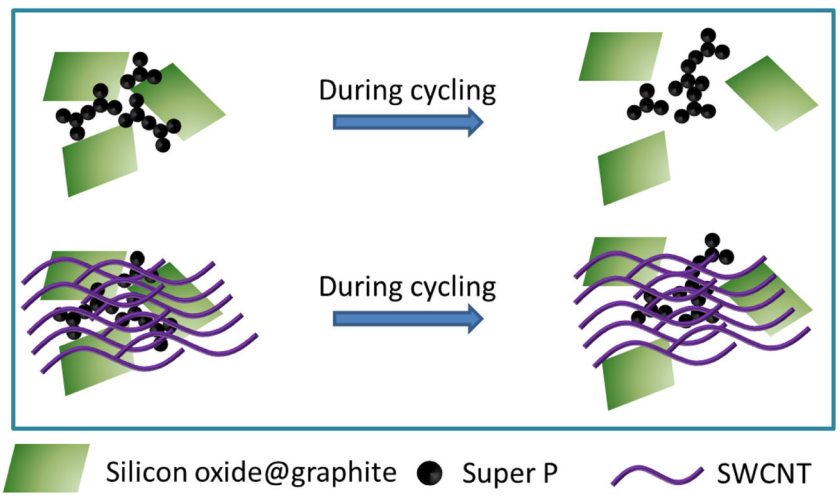


**Fig. 1** Schematics of conductive network for SP and SWCNT

**Table 1** The composition of SiO/C anode electrodes prepared in this work

| Samples | Anode | Binder | Conductive additive | |
|---|---|---|---|---|
| | | | Super P | SWCNT |
| SP | 93.40% | 2.60% | 4.00% | – |
| SWCNT-A | 95.40% | 2.60% | 1.50% | 0.50% |
| SWCNT-B | 95.40% | 2.60% | 1.20% | 0.80% |

as-prepared sample. The probe diameter was approximately 14 mm (area is 1540.25 $mm^2$). The nano-indentation tests were measured using G200 nano indentation system.

### Cell assembly and electrochemical testing

Each pouch cell was assembled via lamination process. It contains 13 layer anode (8.5 cm × 15.6 cm in size) and 12 layer cathode (8.4 cm × 15.3 cm in size), filled with around 37.3 g electrolyte (1.05 mol/L LiPF6 including ethylene carbonate-ethyl methyl carbonate-diethyl carbonate (EC/EMC/DEC, 3:5:2 by weight) with addition of 1 wt% vinylene carbonate (VC), 1 wt% propylene sulfite (PS), 5 wt% fluorinated ethylene carbonate (FEC). The basic electrochemical characterizations of cathode and anode were tested in coin cells. A LAND battery was used to perform the charge–discharge performances of the coin cells with the voltage range of 0.01–1.5 V vs. $Li/Li^+$ for anode and 2.75–4.2 V vs. $Li/Li^+$ for cathode at room temperature, respectively. For the A/C impedance measurements, the frequency ranged from 0.01 Hz to 100.00 kHz. The rate and cycling performance for pouch cells were carried out between 2.75 and 4.2 V on a BTS-5V/50A battery-testing instrument (Kinte Industrial Co., Ltd., China) at room temperature. The hybrid pulse power characterization (HPPC) test was used to assess the resistance of cells at 20%, 50%, and 90% state-of-charge (SOC) [25].

## Results and discussions

Figure 2 a and c show that SP conductive additive distributes inhomogeneously in the bare SiO/C sample and large amounts of SP aggregates between the micrometer-sized active particles, resulting in a long electron transport pathway through SiO/C anode material to the SP conductive additive. In contrast, SWCNT conductive additives are effectively dispersed on overall surface of primary SiO/C particles and no obvious aggregates were found, as shown in Fig. 2 b and d. This 3D SWCNT network and intimate contact between SWCNT and primary SiO/C particles are beneficial to form extremely efficient electron transport pathways.

Galvanostatic charge–discharge measurements were employed to investigate the fundamental electrochemical performances of cathode and anode materials. The initial charge and discharge curves of cathode are plotted in Fig. S1. And its first discharge capacity is 205.2 mAh $g^{-1}$ at 0.1 C under 25 °C over the potential window of 2.75–4.2 V. Figure 3 a shows the typical lithiation/delithiation profiles for SP and SWCNT adding SiO/C materials under the same rate over the voltage range of 0.01–1.5 V. The first charge capacity is

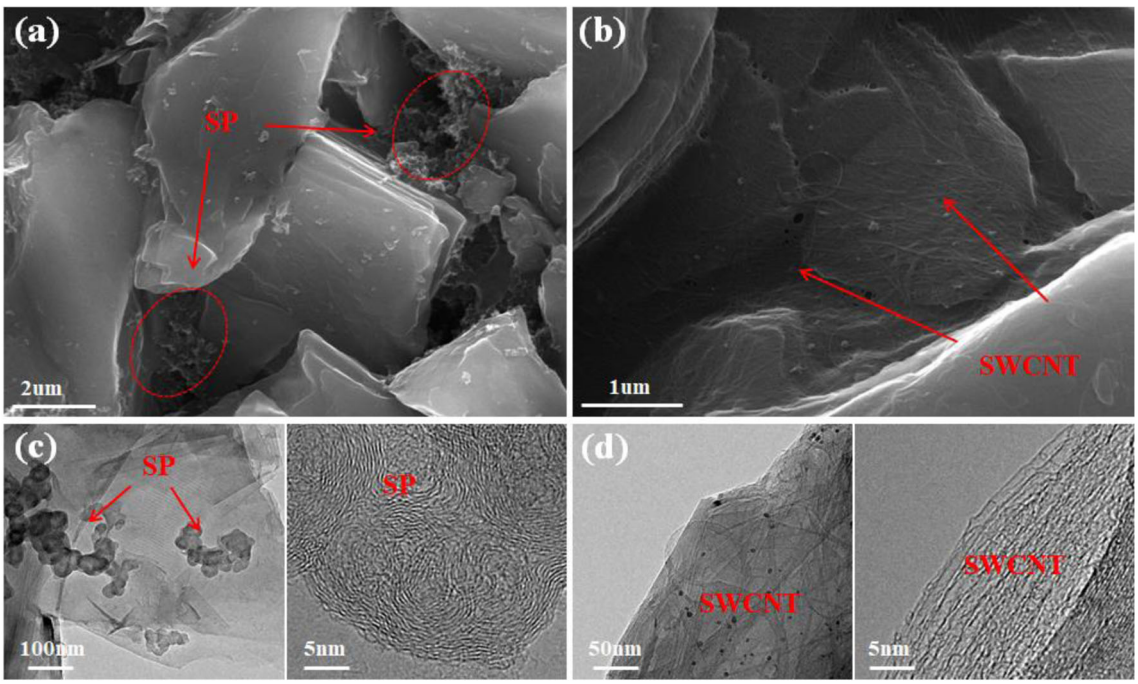


**Fig. 2** FESEM and TEM images of SiO/C anode electrode with SP additive sample (**a**, **c**) and SWCNT-B (**b**, **d**)

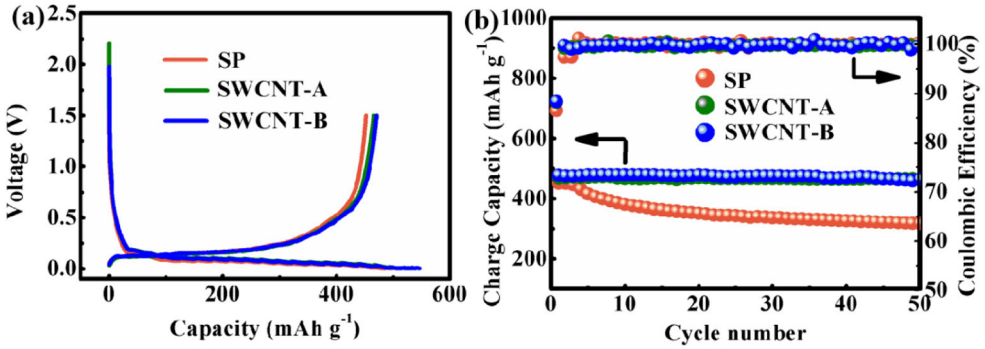


**Fig. 3** Galvanostatic charge–discharge voltage profiles (**a**) and cycling performance (**b**) for SP, SWCNT-A, and SWCNT-B at 0.1 C rate over the voltage window of 0.01–1.5 V (versus $Li/Li^+$)

452.2 mAh $g^{-1}$, 468.7 mAh $g^{-1}$, and 477.1 mAh $g^{-1}$, with an initial columbic efficiency of 86.5%, 88.2%, and 88.4% for SP, SWCNT-A, and SWCNT-B, respectively. The improved reversible capacity and initial coulomb efficiency of SWCNT sample can be ascribed to provide more transmission routes for lithium-ion and electron. As presented in Fig. 3b, the reversible capacity of SP sample decreases to 317.4 mAh $g^{-1}$, which corresponds to 70.2% retention of initial capacity during 50 cycles. However, the cycling performance of SWCNT-adding SiO/C sample is better than that of SP sample. For example, the SWCNT-B sample has charge specific capacity of 464.6 mAh $g^{-1}$, with a capacity retention of 97.4% at the same cycles.

As shown in Fig. 4a, the film resistance was measured to be 3.17, 0.82, and 0.74 Ohm·$cm^2$ for SP, SWCNT-A, and SWCNT-B samples, respectively. The film resistance value of the SWCNTs sample was approximately a quarter of that of SP electrode, indicating the effective electron networks formed by SWCNT additives. The charging DCR for LNCM//SiO/C pouch cell at 20%, 50%, and 90% SOC were measured as shown in Fig. 4b. Due to the highly efficient 3D conductive network in SWCNT-A and SWCNT-B samples, their corresponding DCR values are smaller than that of the SP electrode at all the three SOC states. For example, the resistances at 50% SOC are decreased by 30%.

In order to further understand how SP and SWCNT conductive additive affect the impedance behavior of cell, EIS studies for fresh coin cell were carried out and the Nyquist plots are illustrated in Fig. 4c. All Nyquist plots are composed of one semicircle and a sloping line. The semicircle can be attributed to the charge-transfer resistance ($R_{ct}$). A suitable electric equivalent circuit (EEC) was carried out to fit EIS data and the fitting parameters are listed in Table 2. The $R_{ct}$ values of SWCNT-A cell (37.95 Ω) and SWCNT-B cell (33.95 Ω) are significantly

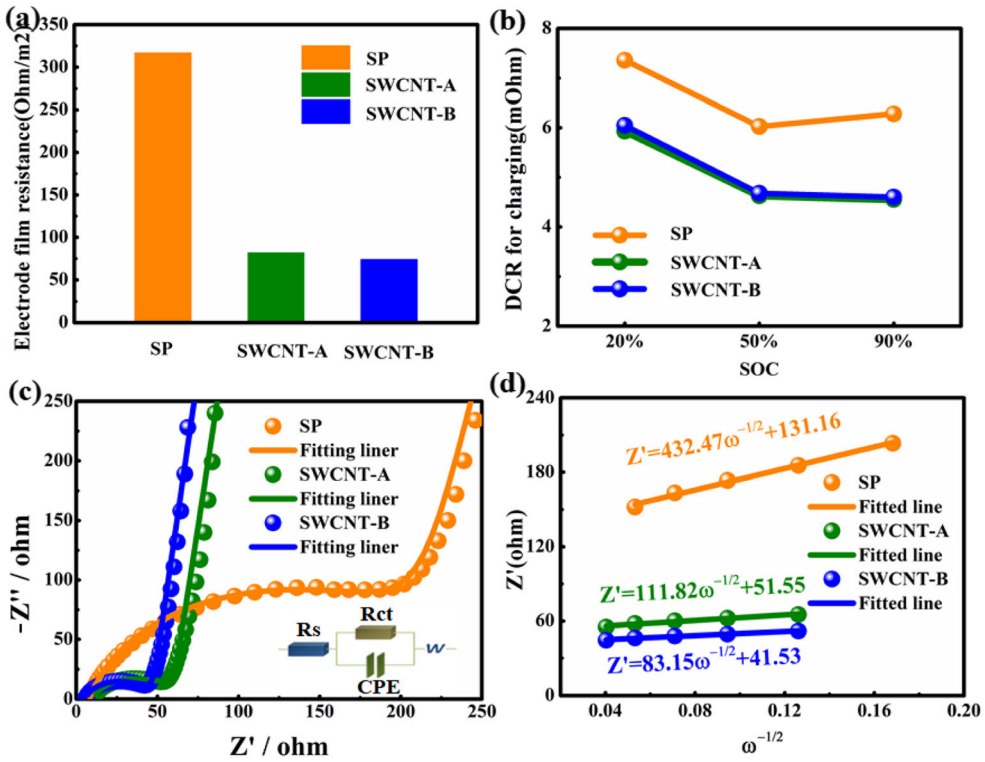


**Fig. 4** The film resistance of electrode containing SP and SWCNT as conductive additives (**a**), DCR of cells using the silicon oxide@graphite composite electrodes containing SP and SWCNTs as conductive additives (**b**), electrochemical impedance spectra profiles and liner fitting of Z′ vs. $w^{-1/2}$ for SP, SWCNT-A, and SWCNT-B (**c**, **d**)

**Table 2** Typical fitting parameters for SP, SWCNT-A, and SWCNT-B

| Samples | $R_s$ (Ω) | $R_{ct}$ (Ω) | $D_{Li}$ ($cm^2\ s^{-1}$) |
|---|---|---|---|
| SP | 8.13 | 183.6 | $2.33 \times 10^{-16}$ |
| SWCNT-A | 10.61 | 37.95 | $3.49 \times 10^{-15}$ |
| SWCNT-B | 5.66 | 33.95 | $6.32 \times 10^{-15}$ |

smaller than those of SP cell (183.6 Ω). The low $R_{ct}$ value of SWCNT electrode indicates its better electronic conductivity and kinetics characteristic than that of SP electrode, which are good consistent with the results in Fig. 4a and b.

Furthermore, the diffusion coefficient of lithium-ion ($D_{Li}^+$) was investigated according to the below equation [16, 26–31] and listed in Table S2:

$$D_{Li}^+ = R^2T^2/2A^2n^4F^4C^2\sigma^2 \quad (1)$$

where R is the gas constant, T is the room temperature in our work, A is the area of anode electrode, n is the number of transferred electrons, F is the Faraday constant, C is the molar concentration of $Li^+$ in anode electrode, and σ is the Warburg coefficient that calculated from the slope of $Z \sim \omega^{-1/2}$ plot. As shown in Fig. 4d, the $D_{Li}^+$ is calculated to be $2.33 \times 10^{-16}$ $cm^2\ s^{-1}$, $3.49 \times 10^{-15}$ $cm^2\ s^{-1}$, and $6.32 \times 10^{-15}$ $cm^2\ s^{-1}$ for SP, SWCNT-A, and SWCNT-B samples, respectively. The $Li^+$ diffusion coefficient of the SWCNT electrode was approximately one order magnitude larger than that of SP sample. The improvement of $D_{Li}^+$ for SWCNT could be ascribed to as follows [32, 33]: (1) a high surface area for tethering of electroactive compounds, (2) enhanced $Li^+$ conductivity and transport within the composite due to well-directed 1D conductive pathways, and (3) reduced diffusion length due to nanometric structure (Fig. S2).

For understanding the effect of SWCNT conductive additive on the charge and discharge rate performance, the pouch cells were measured under 0.5 C, 1.0 C, 2.0 C, 3.0 C, and 4.0 C, as depicted in Fig. 5 a–f. Herein, the charge efficiency refers to the ratio of charge capacity at constant current stage to the charge capacity at constant current-constant voltage stage. And the discharge efficiency is regarded as the ratio of discharge capacity at corresponding C rates to the discharge capacity at 0.5 C. All cells demonstrate similar configuration for charge/discharge efficiencies at 0.5 C. The SWCNT conductive additive has a good effect on rate performance with increasing C rate. In order to further identify an effect, both charge constant current ratio and discharge capacity retention

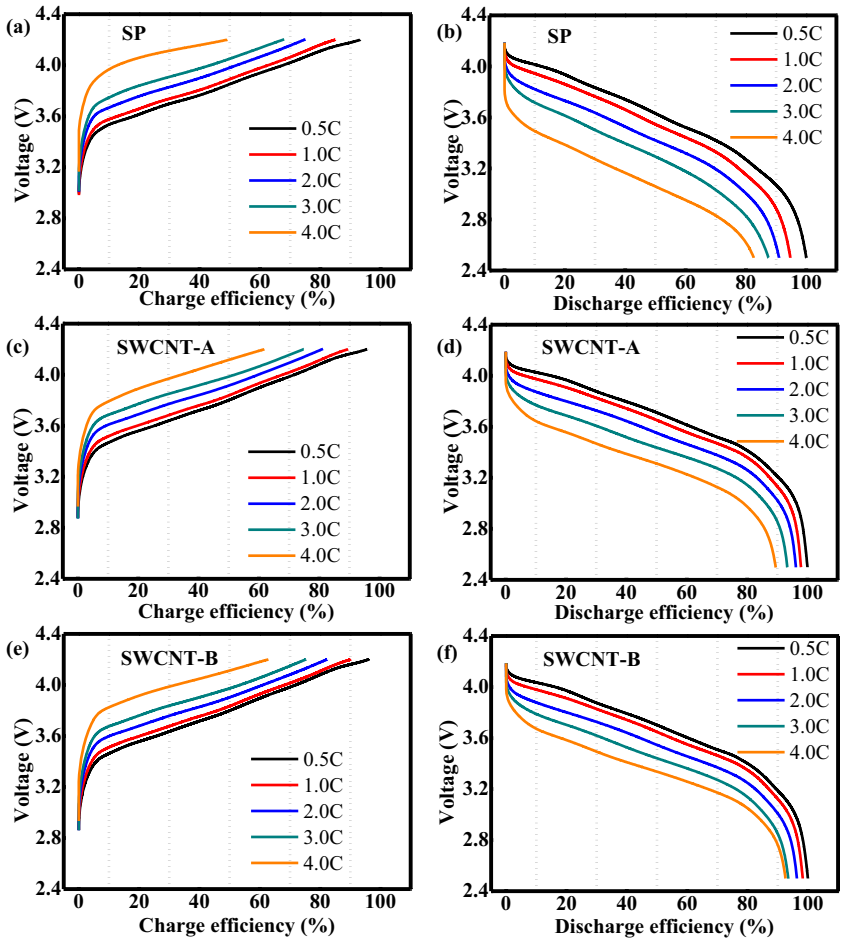


**Fig. 5** The typical charge and discharge curves of full cells at different C rates: SP (**a**, **b**), SWCNT-A (**c**, **d**), SWCNT-B (**e**, **f**)

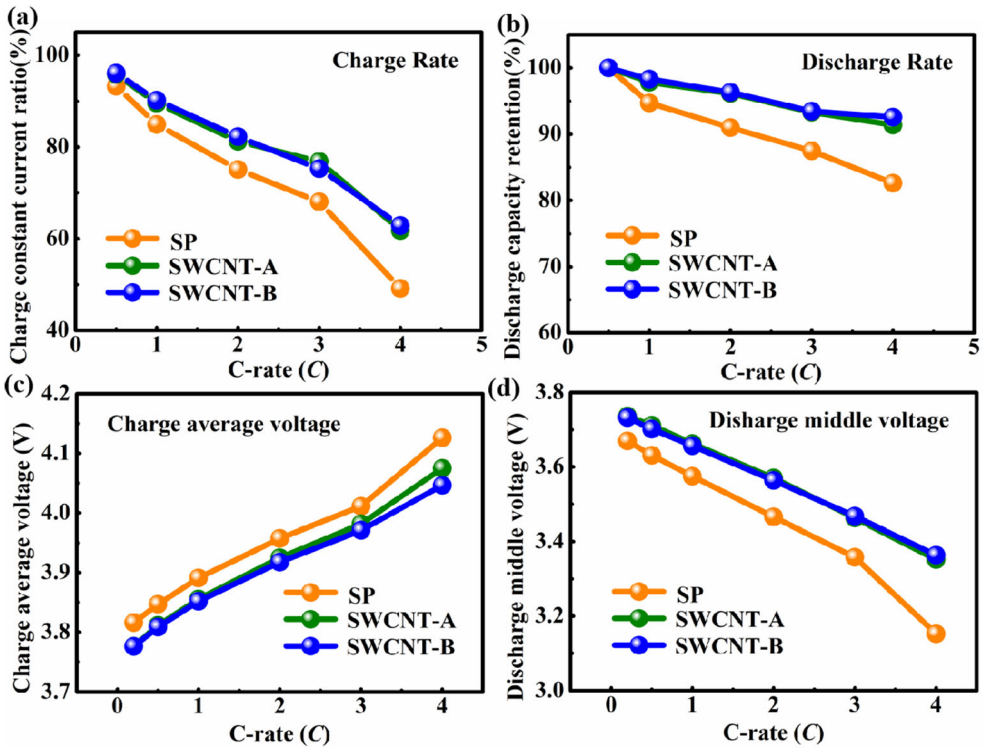


**Fig. 6** The charge constant current ratio (**a**), discharge capacity retention (**b**), average charge voltage (**c**), and discharge middle voltage (**d**) at different C rates

with different C rate are listed in Fig. 6 a and b. There is no obvious difference at 0.5 C between SP and SWCNT electrode. However, a remarkable deviation was illustrated above 1 C with the SP sample decreasing quickly with the improvement of C rate. The result indicates that rate capability of SWCNT electrode has significantly improved. The SWCNT can provide 3D conductive framework, which facilitates electron and ion transport and reduces charge-transfer resistance, especially for high rates. In addition, the benefits of SWCNT can also be evidenced by the charge average voltage and discharge middle voltage as illustrated in Fig. 6 c and d. The average charge voltages for SWCNT-A and SWCNT-B are almost the same and constantly lower than SP sample. And the discharge middle voltage shows the decreasing trend for three type cells. However, the downward trend is more obvious for SP sample.

The cycling stability of the active materials is one of the important demands for practical application. To investigate the stability, the three type samples for pouch cells were tested at 1 C for 600 cycles. As shown in Fig. 7, the three samples for SP, SWCNT-A, and SWCNT-B exhibited a similar initial discharge capacity of 12.3 Ah. However, the SP sample suffers from worse capacity fading, which remains only 10 Ah after 600 cycles. When SWCNT is added, the cycling stability is much improved for SWCNT-A and SWCNT-B sample with approximately 90.3% capacity retention, which is obviously higher than the SP sample (i.e., 81.1%).

The electrode swelling was characterized by the inspection of cross-sectional SEM morphology of electrodes to study why the SWCNT electrodes showed better cycling performance than the super P sample. As demonstrated in Fig. 8, the thickness of SWCNT-A electrode after 300 cycles is ca.

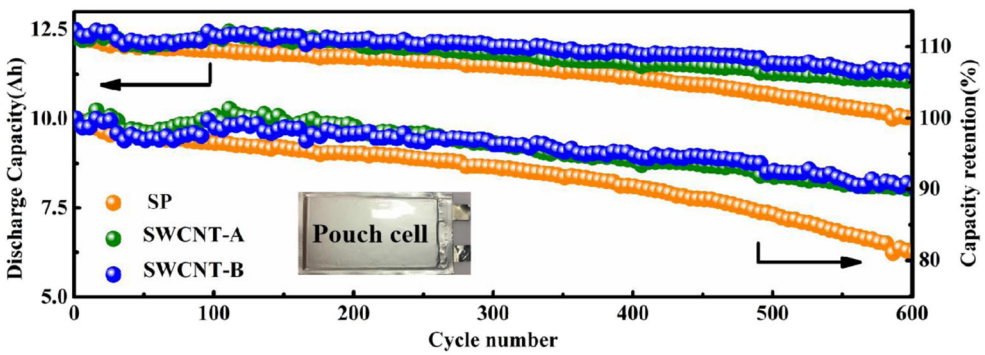


**Fig. 7** Cycling performance for pouch cells

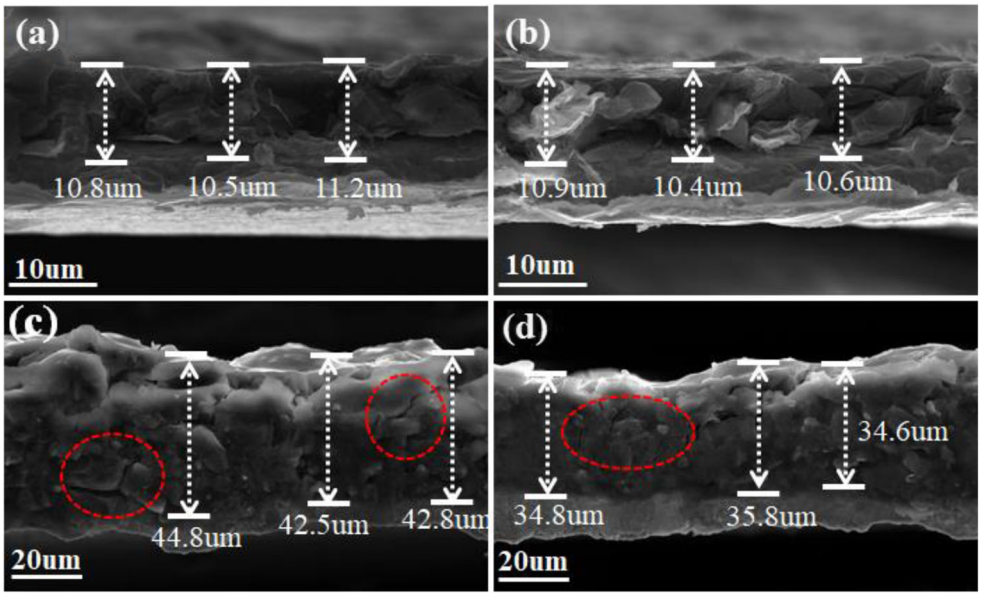


**Fig. 8** The SEM cross section morphology of electrode SP (**a**) and electrode SWCNT-A (**b**) before cycle; electrode SP (**c**) and electrode SWCNT-A (**d**) after 300 cycles

35.1 μm, ca. 231% of the original thickness (ca. 10.6 μm). In sharp contrast, the super P electrode has ca. 302% of expansion (43.4 μm) after 300 cycles. Moreover, the discrete cracks for SP cycled electrode have been observed (Fig. S3b) in comparison with cycled SWCNT-A electrode, which might be caused by greater expansion. Meanwhile, partial active anode materials of SP electrode after cycling were peeled off from substrate, which is worse than that of SWNCT electrode (Fig. S3a,c). The possible reason is that the SWCNT electrode has better mechanical properties than that of SP electrode. The mechanical properties of super P and SWCNT electrode are therefore measured using nano-indentation test. As shown in Fig. S4, the maximum force of SWCNT electrode is approximately 40 mN, which is higher than that of SP electrode (17.8 mN). This result implies that the SWCNT electrode can provide greater tolerance to expansion than that of super P electrode.

## Conclusion

The superior SiO/C composite anodes using SWCNT as a conductive additive were fabricated through an aqueous process. The pouch batteries, using SiO/C anode and LNCM cathode, were produced for the electrochemical capability, including electrochemical impedance spectroscopy, rate, and cycle performance. In comparison with the cells with SP conductive additive, those with SWCNT additive exhibit much higher charge–discharge rate performance above 1 C rate. Furthermore, the cycling results validate that the SWCNT additive can improve capacity retention of the cell to 90.3% after 600 cycles as compared to 81.1% with only SP conductive additive. The improved performance is attributed to that SWCNT not only can significantly improve the conductivity by forming three-dimensional conductive network and fully covering the primary SiO/C particles but also enhance the tolerance of volume expansion.

**Funding information** The financial support was from National Natural Science Foundation of China (51572300) and the Graduate Innovation Project of Central South University (502221908).

## References

1. Ji L et al (2011) Recent developments in nanostructured anode materials for rechargeable lithium-ion batteries. Energy Environ Sci 4(8):2682
2. Tarascon JM, Armand M (2008) Building better batteries. Nature 451(7179):652–657
3. Chu S, Majumdar A (2012) Opportunities and challenges for a sustainable energy future. Nature 488(7411):294–303
4. Goodenough JB, Kim Y (2010) Challenges for rechargeable li batteries†. Chem Mater 22(3):587–603
5. Yang S-q et al (2019) Li4V2Mn(PO4)4-stablized Li[Li0.2Mn0.54Ni0.13Co0.13]O2 cathode materials for lithium ion batteries. Nano Energy 63:103889
6. Zhou CX, Wang PB, Zhang B, Tang LB, Tong H, He ZJ, Zheng JC (2019) Formation and effect of residual Lithium compounds on li-rich cathode material Li1.35[Ni0.35Mn0.65]O2. ACS Appl Mater Interfaces 11(12):11518–11526
7. Zheng J-c et al (2018) In situ formed LiNi0.8Co0.15Al0.05O2@Li4SiO4 composite cathode material with high rate capability and long cycling stability for lithium-ion batteries. Nano Energy 53:613–621
8. Wu L et al (2014) Synthesis and electrochemical properties of x LiMn 0.9 Fe 0.1 PO 4 · y Li 3 V 2 (PO 4 ) 3 /C composite cathode materials for lithium–ion batteries. Electrochim Acta 146:288–294

9. Liu D et al (2019) A cation/anion co-doped Li1.12Na0.08Ni0.2Mn0.6O1.95F0.05 cathode for lithium ion batteries. Nano Energy 58:786–796
10. Etacheri V et al (2011) Challenges in the development of advanced li-ion batteries a review. Energy Environ Sci 4:3243–3262
11. An C et al (2019) Graphene wrapped FeSe2 Nano-microspheres with high Pseudocapacitive contribution for enhanced Na-ion storage. Adv Energy Mater 9(18):1900356
12. Tang LB, Zhang B, An CS, Li H, Xiao B, Li JH, He ZJ, Zheng JC (2019) Ultrahigh-rate behavior anode materials of MoSe2 Nanosheets anchored on dual-heteroatoms functionalized Graphene for sodium-ion batteries. Inorg Chem 58(12):8169–8178
13. Su X et al (2014) Silicon-based Nanomaterials for Lithium-ion batteries a review. Adv Energy Mater 4(1):1–23
14. Ling M et al (2015) Dual-functional gum arabic binder for silicon anodes in lithium ion batteries. Nano Energy 12:178–185
15. Song F et al (2018) High-performance phosphorus-modified SiO/C anode material for lithium ion batteries. Ceram Int 44(15):18509–18515
16. Xia M et al (2019) Improving the electrochemical properties of a SiO@C/graphite composite anode for high-energy lithium-ion batteries by adding lithium fluoride. Appl Surf Sci 480:410–418
17. Tang R et al (2016) How a very trace amount of graphene additive works for constructing an efficient conductive network in LiCoO 2 -based lithium-ion batteries. Carbon 103:356–362
18. Lin Q, Harb JN (2004) Implementation of a thick-film composite li-ion microcathode using carbon nanotubes as the conductive filler. J Electrochem Soc 151(8):A1115–A1119
19. Landi BJ et al (2009) Carbon nanotubes for lithium ion batteries. Energy Environ Sci 2(6):638–654
20. De Volder MF et al (2013) Carbon nanotubes: present and future commercial applications. Science 339(6119):535–539
21. Lim LY et al (2015) Operando X-ray studies of crystalline Ge anodes with different conductive additives. J Phys Chem C 119(40): 22772–22777
22. Sheem K, Lee YH, Lim HS (2006) High-density positive electrodes containing carbon nanotubes for use in li-ion cells. J Power Sources 158(2):1425–1430
23. Luo S, Wang K, Wang J, Jiang K, Li Q, Fan S (2012) Binder-free LiCoO2/carbon nanotube cathodes for high-performance lithium ion batteries. Adv Mater 24(17):2294–2298
24. Westphal BG et al (2017) Influence of high intensive dry mixing and calendering on relative electrode resistivity determined via an advanced two point approach. Journal of Energy Storage 11:76–85
25. Abraham DP et al (2010) Performance of high-power lithium-ion cells under pulse discharge and charge conditions. Int J Energy Res 34(2):190–203
26. Xia M et al (2019) Enhancing the electrochemical performance of micron-scale SiO@C/CNTs anode via adding piezoelectric material BaTiO3 for high-power lithium ion battery. J Alloys Compd 800: 116–124
27. Zuo D-c et al (2019) Synthesis of sandwich-like structured Sn/SnOx@MXene composite through in-situ growth for highly reversible lithium storage. Nano Energy 62:401–409
28. An C-S et al (2019) Binder-free carbon-coated TiO2@graphene electrode by using copper foam as current collector as a high-performance anode for lithium ion batteries. Ceramics International 45(10):13144–13149
29. Zhong S, Wu L, Liu J (2012) Sol–gel synthesis and electrochemical properties of 9LiFePO4·Li3V2(PO4)3/C composite cathode material for lithium ion batteries. Electrochim Acta 74:8–15
30. Liu Y et al (2018) Enhanced electrochemical performance of li-rich layered cathode materials by combined Cr doping and LiAlO2 coating. ACS Sustain Chem Eng 7(2):2225–2235
31. Zheng S et al (2019) Electrochemistry and redox characterization of rock-salt-type lithium metal oxides Li1+z/3Ni1/2-z/2Ti1/2+z/6O2 for li-ion batteries. J Alloys Compd 773:1–10
32. Dimesso L et al (2012) Developments in nanostructured LiMPO4 (M = Fe, co, Ni, Mn) composites based on three dimensional carbon architecture. Chem Soc Rev 41(15):5068–5080
33. Gong C et al (2016) Advanced carbon materials/olivine LiFePO 4 composites cathode for lithium ion batteries. J Power Sources 318: 93–112